Control Volume Approach for Determining Effect of Hartman Number, Nanoparticle Volume Fraction and Suction Parameter on MHD Nanofluid Flow over Stretched Surface

Virginia Mwelu Kitetu[1], Thomas Tony Mboya Onyango[2], Jackson Kioko Kwanza[3]

[1]*Department of Mathematics and Actuarial Science, Catholic University of Eastern Africa*
[2]*Department of Industrial and Engineering Mathematics, Technical University of Kenya*
[3]*Pure and Applied Mathematics, Jomo Kenyatta University of Agriculture and Technology*

***Abstract:* - Currently, numerous studies are being conducted on nanofluids for the benefits associated with low energy costs and less negative environmental impact in industry and society. In the studies, water is commonly used as base for nanofluids in heat transfer applications due to its ability and availability for heat transport. In most of these investigations influence of nanoparticles has been analyzed to determine enhancement of energy transfer on stretched sheets. In this research, magneto hydrodynamic (MHD) flow of a nanofluid over a porous straight stretching sheet with water equally as the base fluid and either copper or silver as nanoparticles is examined and discussed. The physical problem is modeled using systems of unsteady non-linear differential equations (DEs) subject to prescribed boundary and initial conditions, which are then studied using finite volume approach. The effect of nanoparticle volume fraction values, Hartmann number and suction parameter on velocity, temperature and concentration profiles is discussed. Results show that suction enhances velocity and increase in values of nanoparticle volume fractions decrease velocity of nanofluid**

***Key words:* Hartmann number, suction parameter, nanoparticle volume fraction, finite volume approach.**

I. INTRODUCTION

Nanometer-sized particles can be suspended in industrial heat transfer fluids such as water, ethylene glycol, or oil to produce a new class of engineered fluids with high thermal conductivity. Thermal conductivities of most solid materials are higher than those of liquids, therefore thermal conductivities of particle fluid mixtures are expected to increase. Fluids with higher thermal conductivities would have potentials for many thermal management applications. Due to the very small size of the suspended particles, nanoparticle fluid mixtures could be suitable as heat transfer fluids in many existing heat transfer devices, including those miniature devices in which sizes of components and flow passages are small. Many researcher have analyzed flow problems related to nanofluid on a stretching surface and properties of nanofluid: Lee *et al,* (1999) studied the room temperature thermal conductivity of water as well as ethylene glycol based nanofluids consisting of Aluminium oxide (38.5nm) and Copper oxide (23.6nm) nanoparticles. Results showed that copper nanofluid has high thermal conductivity compared to aluminiun. Xinwei and Xianfan (1999) analyzed thermal conductivity of nanoparticle–fluid mixture. Steady-state parallel-plate method was employed in his study. Aluminium oxide and copper oxide nanoparticles were dispersed in three differently fluids: water, vacuum pump fluid, engine oil, and ethylene glycol. High thermal conductivities of nanoparticle–fluid mixtures than those of the base fluids was noticed from the results. Numerical study of heat transfer for water aluminum nanofluids in a radial cooling system was examined by Roy *et al*, (2004). They used nanoparticle volume fraction of 0.1 and concluded that addition of nanoparticles in the base fluids increased the heat transfer rates. They obtained same results to those of Maiga *et al,* (2006) who also used same model. Free convective heat transfer characteristics of a two dimensional horizontal cylinder and a partially heated rectangular enclosure using nanofluids was examined by Wang *et al,* (2006). Water was used as base fluid and copper, silver, aluminium oxide and titanium with different volume fractions of nanoparticles was put into consideration. Kuang and Angela (2010) analyzed natural convection heat transfer of nanofluids in a vertical cavity by considering non-uniform particle diameter and temperature on thermal conductivity. They focused on natural convection in a cavity filled with aluminium water nanofluid that operates under differentially heated walls. Navier–Stokes and energy equations were numerically solved using Xu's model. Examination of heat transfer rate was studied using parameters of non-uniform nanoparticle size, mean nanoparticle diameter, nanoparticle volume fraction, Prandtl number, and Grashof number. They pointed out that, heat transfer was affected by the size of the nanoparticles. Zi (2011) investigated transient buoyancy-driven convective heat transfer of water-based nanofluids in a bottom-heated isosceles triangular enclosure. He used nano-sized copper oxide particles suspended in water with two different volume fractions. The thermo- physical properties of water in the presence of nanoparticles were predicted and Brownian

motion of nanoparticles were taken into account. Results showed that pitchfork bifurcation appears for relatively high Grashof numbers. Norfifah, Anuar and Loan (2011) studied stagnation-point flow over a stretching or shrinking sheet in a nanofluid. A steady two-dimensional stagnation-point flow of a nanofluid over a stretching/shrinking sheet in its own plane was explored. The stretching or shrinking velocity and velocity of free stream were assumed to vary linearly with the distance from the stagnation point. Copper, alumina, and titania nanoparticle in water-based fluid with Prandtl number (Pr = 6.2) was used. The skin friction coefficient, Nusselt number, and the velocity and temperature profiles were presented graphically and discussed. The solid volume fraction on the fluid flow and heat transfer properties were also analyzed. It was found that results for stretching sheet was unique and those of shrinking sheet non-unique. Rama, Reddy and Ali (2011) discussed natural convective boundary layer flow over a horizontal plate embedded in a porous medium saturated with a nanofluid. A boundary layer analysis was presented for the natural convection past a horizontal plate in a porous medium saturated with a nanofluid. Numerical results for friction factor, surface heat transfer rate and mass transfer rate were presented for parametric variations of the buoyancy ratio parameter, Brownian motion parameter, thermophoresis parameter and Lewis number. The dependency of the friction factor, surface heat transfer rate (Nusselt number) and mass transfer rate on these parameters were discussed. Sohail and Changhoon (2012) discussed boundary layer flow of nanofluid over an exponentially stretching surface**.** Effect Brownian motion parameter and thermophoresis parameter on steady boundary layer flow of nanofluid over an exponential stretching surface was investigated analytically. Using similarity transformations nonlinear coupled partial differential equations were simplified and the reduced equations solved analytically using homotopy analysis method (HAM). HAM was found to be convergent and h-curve was plotted. Impact of suction injection parameter, Lewis number, the Brownian motion parameter and thermophoresis parameter on velocity, temperature and concentration was discussed. An interesting work on nanoparticle analysis for steady blood flow of Jeffrey fluid with stenosis with new analytical techniques was investigated by Nadeem, Ijaz and Akbar (2013).They examined effects of heat transfer when nanoparticle fraction was taken into account. Since gravitational effects were put into consideration the tube placed vertically upward. The governing equation were non-dimensionalized and results of simplified equations obtained analytically using homotopy perturbation method (HPM) and a domain decomposition method (DDM). Graphs of velocity profile, nano concentration profile, resistance impedance, wall shear stress, temperature profile, wall shear stress at the stenos is throat and stream lines were drawn. Hayata *et al*, (2014) analyzed MHD flow of nanofluids over an exponentially stretching sheet in a porous medium with convective boundary conditions. Steady MHD flow of viscous nanofluid due toa permeable exponentially stretching surface was explored. The porous space was filled by an incompressible fluid, water was used as base fluid and nanoparticles of copper, silver, alumina and titanium oxide were used. Water was treated as a base fluid. Similarity transformations reduced non-linear PDEs governing the flow to ODEs. The ODEs were solved for the development of series solutions. Convergence of the obtained series solutions was explicitly discussed. Syed, Rizwan and Sohail (2014) studied model-based analysis of micropolar nanofluid flow over a stretching surface. The study used compatible models to deal with the effects of copper and silver nanoparticles. Water and Kerosene were used as base fluids. Both governing equations and boundary equations were reduced into system of coupled nonlinear ordinary differential equations and solved using Runge-Kutta method. Numerical results were in agreement with published data hence accurate. Magneto nanofluid flow with heat transfer past a stretching surface for the new heat flux model was discussed by Noreen, Beg and Khan (2016). A mathematical model for steady, laminar, MHD, incompressible nanofluid flow, heat and mass transfer from a stretching sheet was developed. Khalil, Kambiz and Marilyn (2003) investigated buoyancy-driven heat transfer enhancement in a two-dimensional enclosure utilizing nanofluids. Flow parameter by name solid particle was considered to have effect on heat transfer performance of nanofluids inside the enclosure. Governing equations were solved using the finite volume approach along with the alternating direct implicit procedure. The method was found robust and accurate. Previously published work on special cases were in excellent agreement with numerical solution obtained in this study. Eiyad and Ali (2010) studied mixed convection flow in a lid-driven inclined square enclosure filled with a nanofluid. They focused on the numerical modeling of steady laminar mixed convection flow in a lid driven inclined square enclosure filled with water aluminium nanofluid. The left and right walls of the enclosure were kept insulated while the bottom and top walls were maintained at constant temperatures with the top surface being the hot wall and moving at a constant speed. The developed equations were given in terms of the stream function vortices formulation and were non-dimensionalized and then solved numerically subject to appropriate boundary conditions by a second-order accurate finite-volume method. Zoubair, Abderrahim and Rachid (2017) researched on finite volume analysis of free convection heat transfer in a square enclosure filled by copper-water nanofluid containing different shapes of heating cylinder. They examined numerically natural convection heat transfer of a Cu-water nanofluid in square enclosure containing a central heating cylinder. A two-dimensional solution for natural convection was obtained using the finite volume method with Semi-Implicit Pressure Linked Equations (SIMPLE) algorithm. FVM results were found to be stable.

From the foregoing literature review, what many of the researches carried out shows that MHD nanofluid flow to a stretching surface has not been explored much and the few who have ventured into stretching surface did not pay

attention to a porous linearly stretching surface and did not consider unsteady parameter. Also different methods have been used by researchers to solve problems but in this study FVM was used.

II. DESCRIPTION AND FORMULATION

2.1 Description of problem

In the current study, consider unsteady laminar MHD mixed convective nanofluid flow as a result of porous linearly stretching surface situated at x axis with stretching velocity $u = bx$, where b is a constant: For stretching surface $b > 0$ and for a shrinking surface $b < 0$. Let suction velocity be $v = v_w$ the temperature at the wall is $T = T_w$ and nanoparticle concentration at the stretching surface is $C = C_w$. The temperature of the free stream nanofluid is $T = T_\infty$ and the ambient concentration is C_∞. The x- axis is along the stretching surface and y direction is orthogonal to the stretching surface. The flow experiences magnetic force.

The initial and boundary conditions are respectively:

$$u = 0, v = 0, T = T_w, C = C_w \; at \; t < 0,$$
$$u = U_w = bx, \;\; v = v_w, \;\; T = T_w, \;\; C = C_w : y = 0, t \geq 0$$
$$u = U_\infty = b_\infty x, \;\; v = 0, \;\; T = T_\infty, \;\; C = C_\infty : y \to \infty, t \geq 0'$$

where $v_w < 0$ is suction velocity while $v_w > 0$ is blowing velocity and b_∞ denotes stagnation flow rate parameter.

The properties of nanofluid are defined by Haroun *et al.*, (2015) [8]

$$\mu_{nf} = \frac{\mu_f}{(1-\Phi)^{2.5}}, k_{nf} = k_f\left(\frac{k_s + k_f + 2\Phi(k_s - k_f)}{k_s + 2k_f + \Phi(k_s - k_f)}\right), (\rho c_p)_{nf} = (1-\Phi)(\rho c_p)_f + \Phi(\rho c_p)_s, \rho_{nf} = (1-\Phi)\rho_f + \Phi\rho_s, \Phi_0 = (1-\Phi)^{2.5}\left(1 - \Phi + \Phi\left(\frac{\rho_s}{\rho_f}\right)\right), \Phi_a = \left(1 - \Phi + \Phi\frac{(\rho c_p)_s}{(\rho c_p)_f}\right)$$

where the subscripts f denote base fluid while s represent the nanoparticle. In this study Φ represent nanoparticle volume fraction. The thermal properties of base fluid and nanoparticle are in the table below.

Table1: Thermal physical properties of pure water, copper and silver nanoparticles

Physical properties	Base fluid (water)	Copper	Silver (Ag)
c_p(j/kgk)	4179	385	235
$\rho(kg/m^3)$	997.1	8933	10500
$k(w/mk)$	0.613	401	429

2.2 Governing equations

Velocity, temperature and concentration within the boundary layer are governed by continuity, momentum, thermal energy and concentration equations listed below.

$$\frac{\partial u}{\partial x} + \frac{\partial v}{\partial y} = 0. \quad (1)$$

$$\frac{\partial u}{\partial t} + u\frac{\partial u}{\partial x} + v\frac{\partial u}{\partial y} = -\frac{1}{\rho_{nf}}\frac{\partial p}{\partial x} + \vartheta_{nf}\frac{\partial^2 u}{\partial y^2} + g_a B_T(T - T_\infty) + g_a B_C(C - C_\infty) - \sigma {B_0}^2 u. \quad (2)$$

$$\frac{\partial T}{\partial t} + u\frac{\partial T}{\partial x} + v\frac{\partial T}{\partial y} = \alpha_{nf}\frac{\partial^2 T}{\partial y^2} + \frac{\rho_f D_m k_T}{C_s \rho_{nf}(c_p)_{nf}}\frac{\partial^2 C}{\partial y^2} + \frac{Q}{\rho_{nf}(c_p)_{nf}}(T - T_\infty). \quad (3)$$

$$\frac{\partial C}{\partial t} + u\frac{\partial C}{\partial x} + v\frac{\partial C}{\partial y} = D_m\frac{\partial^2 C}{\partial y^2} + \frac{D_m k_m}{T_m}\frac{\partial^2 T}{\partial y^2} - R(C - C_\infty). \quad (4)$$

where u, v, T and C denote velocity component along x-axis, velocity component along y-axis, temperature and concentration respectively. In the free stream momentum equation (2) reduces to:

$$\frac{1}{\rho_{nf}}\frac{\partial p}{\partial x} = -U_\infty\frac{dU_\infty}{dx} - \sigma\frac{B_0^2}{\rho_{nf}}U_\infty \quad (5)$$

Substituting equation (5) into equation (2) momentum equation simplifies to:

$$\frac{\partial u}{\partial t} + u\frac{\partial u}{\partial x} + v\frac{\partial u}{\partial y} = \vartheta_{nf}\frac{\partial^2 u}{\partial y^2} + U_\infty\frac{dU_\infty}{dx} + (U_\infty - u)\sigma\frac{B_0^2}{\rho_{nf}} + g\beta_T(T - T_\infty) + g_a\beta_C(C - C_\infty). \quad (6)$$

In order to satisfy continuity equation a stream function given by [8]

$$\varphi = \sqrt{b_\infty \vartheta_f \varepsilon}\, x f(\varepsilon, n), \quad (7)$$

is introduced whereby:

$$u = \frac{\partial \varphi}{\partial y}, v = -\frac{\partial \varphi}{\partial x}. \quad (8)$$

III. NON-DIMENSIONALIZING GOVERNING EQUATIONS

Equations (1), (3), (4) and (6) are non-dimensionalized using dimensionless variables; namely dimensionless length along y direction n, dimensionless time ε, dimensionless stream function $f(\varepsilon, n)$, dimensionless temperature $\theta(\varepsilon, n)$ and dimensionless concentration as:

$$y = n\sqrt{\frac{\vartheta_f \varepsilon}{b_\infty}}, \;\; \varepsilon = 1 - e^{b_\infty t}, \;\; f(\varepsilon, n) = \frac{1}{\sqrt{a_\infty \vartheta_f \varepsilon x}}, \;\; \frac{\theta(n)}{g(\varepsilon)} = \frac{T - T_\infty}{T_w - T_\infty} \;\; \frac{\emptyset(n)}{g(\varepsilon)} = \frac{C - C_\infty}{C_w - C_\infty} \quad (9)$$

Using equations (8) and (9) the governing equations (3), (4) and (6) reduces to:

$$f''' + \Phi_0\left[(1-\varepsilon)\frac{n}{2}f'' + \varepsilon\left(-f'^2 + ff'' + 1 + Ha^2(1 - f') + Gr_T\frac{\theta}{g(\varepsilon)} + Gr_C\frac{\emptyset}{g(\varepsilon)}\right)\right] = \Phi_0\varepsilon(1-\varepsilon)\frac{\partial}{\partial\varepsilon}f' \quad (10)$$

$$\theta'' + \frac{k_f}{k_{nf}} pr\Phi_a \left\{\frac{n}{2}(1-\varepsilon)\theta' + \varepsilon[f\theta' + \sigma\theta] + \frac{D_f}{\Phi_a}\emptyset''\right\} = -\frac{k_f}{k_{nf}} pr\Phi_a \varepsilon(1-\varepsilon)\frac{\theta g_\varepsilon}{g}, \quad (11)$$

$$\emptyset'' + Sc\left[\frac{n}{2}(1-\varepsilon)\emptyset' + \varepsilon(f\emptyset' - \gamma\emptyset) + Sr\theta''\right] = -Sc\varepsilon(1-\varepsilon)\frac{\emptyset}{g} g_\varepsilon, \quad (12)$$

where $g_\varepsilon = \frac{\partial g}{\partial \varepsilon} = q$, hence $g = q\varepsilon$ and q is a constant.

The non-dimensionalized boundary conditions are respectively:

$$f(\varepsilon,0) = f_w, f'(\varepsilon,0) = \lambda, \theta(\varepsilon,0) = \varepsilon, \emptyset(\varepsilon,0) = \varepsilon \; at \; n = 0, \varepsilon \geq 0, \quad (13)$$

$$f'(\varepsilon,\infty) = 1, \theta(\varepsilon,\infty) = 0, \emptyset(\varepsilon,\infty) = 0, as \; n \to \infty, \varepsilon \geq 0, \quad (14)$$

where $f_w = -\frac{v_w}{(b_\infty \vartheta_f \varepsilon)^{\frac{1}{2}}}$.

Equations (10), (11) and (12) are simplified further by considering a case where $\varepsilon = 1$ and $t \to \infty$, corresponding to $f(n,1) \approx f(n), \theta(n,1) \approx \theta(n) \; and \; \emptyset(n,1) \approx \emptyset(n)$. In this case equations (10), (11) and (12) reduce to:

$$\frac{d^3 f}{dn^3} + \Phi_0\left[f\frac{d^2 f}{dn^2} - \left[\frac{df}{dn}\right]^2 + 1 + Ha^2\left(1 - \frac{df}{dn}\right) + Gr_T\theta + Gr_C\emptyset\right] = 0. \quad (15)$$

$$\frac{d^2\theta}{dn^2} + \frac{k_f}{k_{nf}} Pr\Phi_a\left(f\frac{d\theta}{dn} + \delta_a\theta\right) + \frac{k_f}{k_{nf}} PrD_f\frac{d^2\emptyset}{dn^2} = 0. \quad (16)$$

$$\frac{d^2\emptyset}{dn^2} + Sc\left(f\frac{d\emptyset}{dn} - \gamma\emptyset\right) + ScSr\frac{d^2\theta}{dn^2} = 0. \quad (17)$$

From the non-dimensionalization the following dimensionless parameters were obtained:

$$Pr = \frac{\vartheta_{nf}}{\alpha_{nf}}, Gr_T = \frac{g\beta_T(T_w - T_\infty)}{b_\infty^2 x}, Gr_c = \frac{D_m K_T(C_w - C_\infty)}{b_\infty^2 x}, Ha^2 = \frac{\sigma {B_0}^2}{b_\infty \rho_{nf}}, \sigma = \frac{Q}{b_\infty(\rho c_p)_{nf}}, D_f = \frac{D_m k_T(C_w - C_\infty)}{C_s(c_p)_f \vartheta_f(T_w - T_\infty)}, sc = \frac{\vartheta_{nf}}{D_m}, \gamma = \frac{R}{b_\infty}, sr = \frac{D_m k_T(T_w - T_\infty)}{T_m \vartheta_f(C_w - C_\infty)}$$

Skin friction, Nusselt number and Sherwood numbers are given by equations (18), (19) and (20) respectively:

$$C_f = -\frac{2}{\rho_f {U_\infty}^2}\frac{U_\infty \mu_f}{(1-\Phi)^{2.5} x}\sqrt{\frac{U_\infty x}{\vartheta_f \varepsilon}} f_{nn}(0,\varepsilon) = -\frac{2}{\sqrt{(1-\Phi)^5}}\frac{f_{nn}(0,\varepsilon)}{\sqrt{\varepsilon Re}}, \quad (18)$$

$$Nu = -\frac{k_{nf}}{k_f}\sqrt{\frac{Re}{\varepsilon}}\theta_n(0,\varepsilon), \quad (19)$$

$$Sh = -\left(\frac{Re_x x}{\varepsilon}\right)^{\frac{1}{2}}\emptyset_n(0,\varepsilon). \quad (20)$$

IV. NUMERICAL TECHNIQUE

$$\frac{1}{\Delta n} f'_{i-1} - \left(\frac{2}{\Delta n} + Ha^2\Delta n\right) f'_i + \frac{1}{\Delta n} f'_{i+1} = -\Phi_0\left\{\frac{f_i}{2}(f'_{i+1} - f'_{i-1}) - (f'_i)^2\Delta n + \Delta n + Ha^2\Delta n + Gr_T\theta_i\Delta n + Gr_C\emptyset_i\Delta n\right\}, \quad (21)$$

$$\frac{1}{\Delta n}\theta_{i-1} + \left(\frac{-2}{\Delta n} + \frac{k_f}{k_{nf}} pr\Phi_a\delta_a\Delta n\right)\theta_i + \frac{1}{\Delta n}\theta_{i+1} = -\frac{k_f}{2k_{nf}} pr\Phi_a f'_i(\theta_{i+1} - \theta_{i-1}) - \frac{k_f}{k_{nf}} prD_f\left(\frac{\emptyset_{i+1}}{\Delta n} - \frac{2\emptyset_i}{\Delta n} + \frac{\emptyset_{i-1}}{\Delta n}\right), \quad (22)$$

$$\frac{1}{\Delta n}\emptyset_{i-1} - \left(\frac{2}{\Delta n} + Sc\gamma\Delta n\right)\emptyset_i + \frac{1}{\Delta n}\emptyset_{i+1} = -\frac{Scf_i}{2}(\emptyset_{i+1} - \emptyset_{i-1}) - ScSr\left(\frac{\theta_{i+1}}{\Delta n} - \frac{2\theta_i}{\Delta n} + \frac{\theta_{i-1}}{\Delta n}\right). \quad (23)$$

V. RESULTS AND DISCUSSION

The graphs in figure 1 and figure 2 are obtained using, $\Phi = 0.3, 0.4, 0.5, f_w = 1, Df = 0.01, \lambda = 0.5, Gr_T = 0.01, Gr_C = 0.01, Pr = 7, sc = 1, sr = 1, \delta_a = 0.1, Ha = 2, \gamma = 0.1, \; \varepsilon = 1, Re = 1$. Results in figures 3, 4, 5and 6 are obtained using table 1 and $\Phi = 0.2, Df = 0.01, \lambda = -2, Gr_T = 0.01, Gr_C = 0.01, Pr = 7, Ha = 2 \; \delta_a = 0.2, sc = 1, sr = 1, , \gamma = 3, \; \varepsilon = 1$ and $Re = 1$

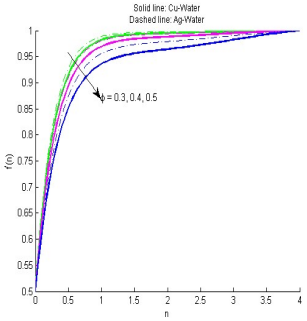

(a)

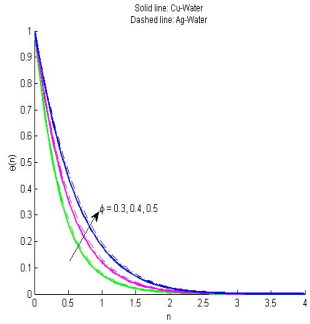

(b)

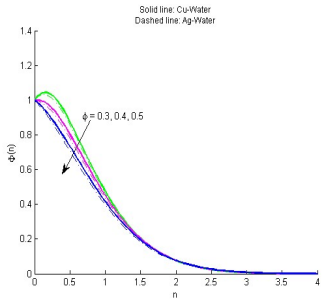

(c)

Figure 1: (a) velocity, (b) temperature and (c) concentration profiles when varying nanoparticle volume fractions

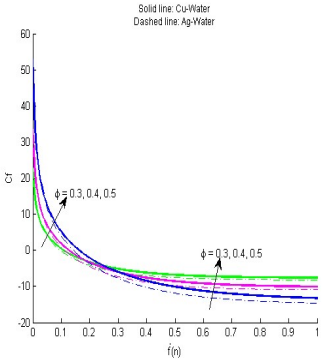

(a)

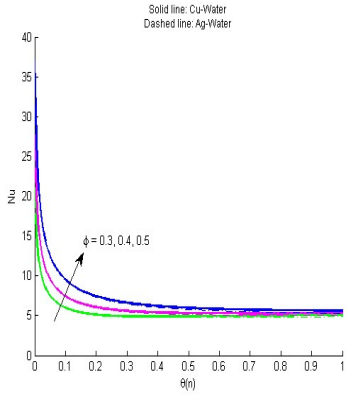

(b)

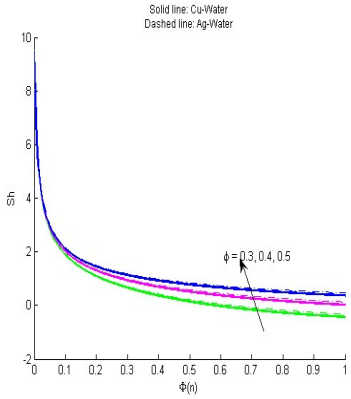

(c)

Figure 2: (a) Skin friction (b) heat transfer and (c) mass transfer coefficients when varying 140anoparticles volume fractions

In figure 1(a), the velocity of nanofluid is reducing with increase of nanoparticles volume fractions. The momentum layer thickness is increasing when nanoparticles volume fraction increases. The velocity of silver-water nanofluid is higher compared to the one of copper-water nanofluid because silver-water nanofluid is less viscous than copper-water.vFrom figure 2(b), temperature is increased when values of 140anoparticles volume fraction is increased since when 140anoparticles volume fraction values are increased, thermal conductivity of nanofluid is increased. As observed from the graphs, temperature distribution of copper- water nanofluid is lower than that of silver- water nanofluid implying that silver has higher thermal conductivity than copper. Using figure 1(c), concentration of nanofluid reduce when 140anoparticles volume fractions amount become greater in size because of surface drag. Consequently, mass transfer is decreased resulting to high concentration gradient at the surface and concentration boundary layer thickness is decreased with increase of volume fractions of 140anoparticles. The concentration of copper-water nanofluid is higher than that of silver- water nanofluid. This is because copper-water is more viscous than silver-water nanofluid. Skin friction coefficient on the surface increase with increasing values of 140anoparticles volume fractions as illustrated in figure 2(a) up to critical point. This is because when 140anoparticles volume fractions are increased, nanofluid become more viscous which results to increased surface drag. From figure 2(b), heat transfer coefficient or Nusselt number increase when 140anoparticles volume fraction values are increasedbecause when 140anoparticles volume fractions are increased, thermal conductivity also increases. This is in agreement with physical properties of nanofluids. It is observed that from figure 2(c) that mass transfer coefficient or Sherwood number increases when the value of 140anoparticles fraction is increased. Copper-water nanofluid experience less rate of mass transfer as compared to silver-water nanofluid.

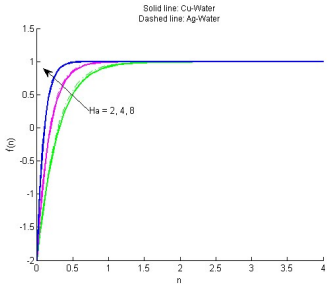

(a)

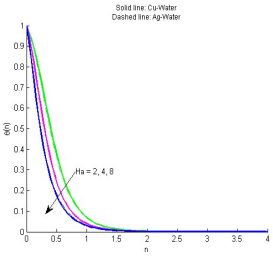

(b)

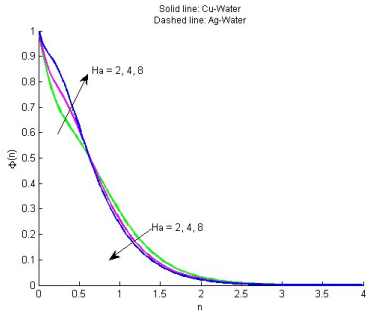

(c)

Figure 3: (a) Velocity, (b) temperature and (c) concentration profiles when Hartmann number is varied

In figure 3 (a), when value of Hartman number is increased also velocity increases. This is because of suction which removes nanofluid from the surface hence decreasing momentum boundary layer thickness and surface drag which offers resistance to the flow. Copper-water nanofluid is slower compared to silver-water nanofluid because silver-water nanofluid is less viscous than copper-water nanofluid. Velocity is increasing with increasing value of n for both nanofluids due to no slip condition. Temperature decrease when Hartmann number is increased as shown in figure 3(b). This is caused by increase of thermal boundary layer thickness and temperature gradients at the surface. Figure 3(c) shows that at the stretching surface concentration increase with increase of Hartman number up to critical point. This is due to increased velocity on the surface as a result of suction hence decreased mass transfer boundary layer thickness and concentration gradients. This results to high mass diffusion on the surface. Beyond critical point concentration decreases because suction effect are neglected since the fluid is not in contact with the stretching surface hence the nanofluid possess free stream concentration.

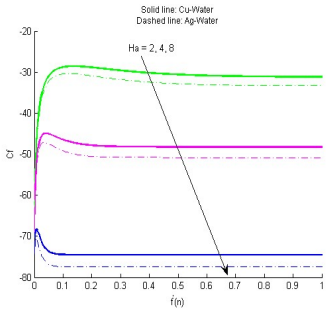

(a)

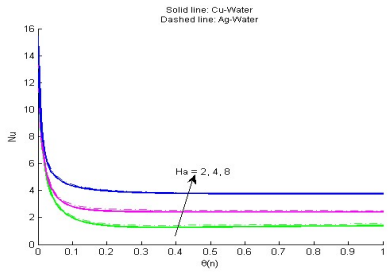

(b)

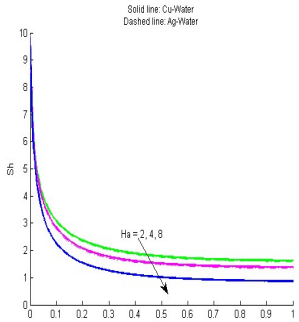

(c)

Figure 4: (a) skin friction, (b) heat transfer and (c) mass transfer coefficients when varying Hartmann number

From figure 4(a), skin friction decrease when Hartmann number is increased due to high velocity of nanofluid which offer less viscous effect to the flow. Silver-water nanofluid exhibit less surface drag than copper-water nanofluid since silver-water nanofluid is faster than copper-water nanofluid. The observation from figure 4(b), is that heat flux increases when Hartmann number is increased. It is observed that silver-water has higher Nusselt number when compared to copper-water nanofluid because copper-water has lower velocity than silver-water nanofluid. From figure 4(c), mass transfer coefficient decrease when Hartmann number rises because of suction which removes fluid from the stretching surface

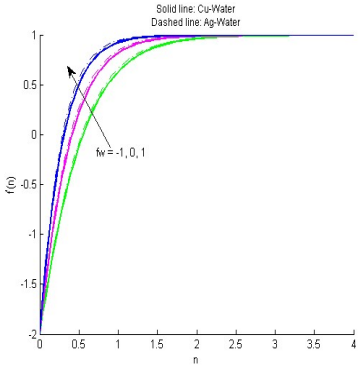

(a)

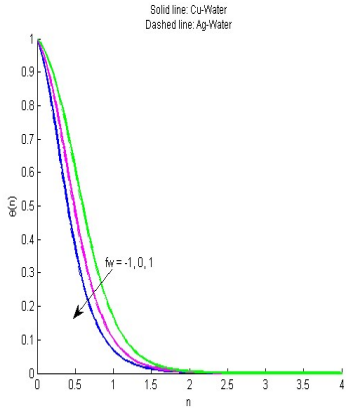

(b)

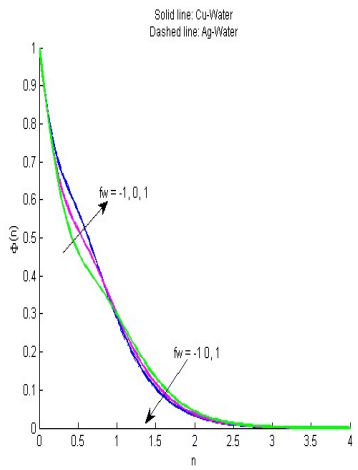

(c)

Figure 5: (a) velocity, (b) temperature and concentration profiles when varying stretching parameter

In figure 5(a), increase in suction parameter increases the velocity of nanofluid. This is because the thickness of velocity boundary layer is reduced by suction which removes nanofluid from the stretching surface. The injection ($f_w = -1$) makes the fluid to enter the system, hence increasing thickness of momentum boundary layer. This makes velocity of nanofluid to decrease for injection. The velocity of copper-water nanofluid is lower than the one of silver-water nanofluid. This is because copper–water nanofluid is more viscous than silver-water nanofluid. Velocity of nanofluid increases with increasing value of n due to no slip condition. Observation from figure 5(b) is that temperature decrease with increase of suction parameter due to suction that make the nanofluid to be removed from the system hence increased thickness of thermal boundary layer. This results to increased temperature differences at the stretching surface. For the case of injection nanofluid is introduced to the system hence increased thermal conductivity. For injection, thickness of thermal boundary layer reduces which results to decreased temperature gradients on the stretching surface. Temperature is decreasing with increasing values of n. From figure 5(c), on the stretching surface concentration is increased with increase of the suction up to the critical value of n. This is caused by the fact that, suction removes nanofluid from the surface hence increasing velocity of on the nanofluid. Beyond the critical point the fluid is not in contact with stretching surface hence viscous effect are neglected, hence concentration is reduced. For the case of injection, on the stretching surface concentration reduce because nanofluid is allowed to enter the system. As a result thickness of concentration layer increases which causes increase in concentration gradient.

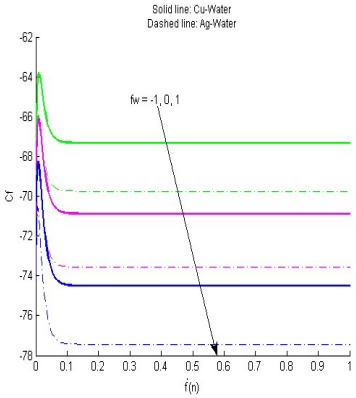

(a)

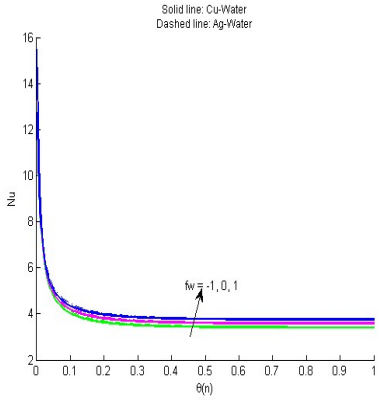

(b)

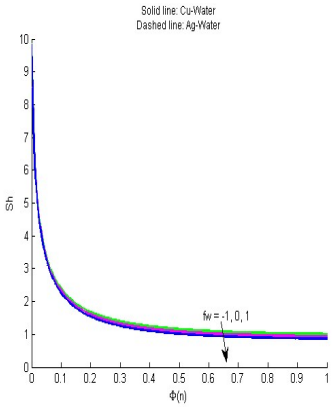

(c)

Figure 6: (a) skin friction, (b) heat transfer and (c) mass transfer coefficients when varying suction parameter

Using figure 6(a), skin friction decrease for the case of suction since suction removes nanofluid from the surface hence increasing the velocity of the nanofluid. As result the surface drag decreases on the stretching surface. For, the case of injection, skin friction increases because injection allows nanofluid to enter the system hence decreases velocity on the surface. As a result surface drag is increased for injection. Skin friction for copper-water nanofluid is higher than that of silver-water because copper-water is more viscous than silver-water nanofluid. For increasing values of suction, Nusselt

number increases slightly from observation in figure 6(b). When injection increases, Nusselt number decreases because there is decrease in thermal conductivity. Figure 6(c), when suction/ injection parameter is increased rate of mass transfer remains constant.

VI. CONCLUSION

Non-dimensiolization of equation governing the flow has been achieved. FVM algorithm for solving the governing equation has been developed. FVM has transformed the coupled momentum, energy and concentration equations to system of linear equations. Nanoparticle volume fraction reduces velocity of nanofluid and increase temperature. Hartman number and suction parameter significantly affect nanofluid velocity and surface drag.

Abbreviation

b: Positive constant

v_w: suction velocity

T_w: Surface temperature

C_w: Surface concentration

T_∞: Ambient temperature

C_∞: Ambient concentration

u: Fluid velocity component along x direction

v: Fluid velocity component along y

ρ_{nf}: Nanofluid density

p: Fluid pressure

ϑ_{nf}: Nanofluid kinematic viscosity

g: Unsteadiness parameter

g_a Gravitational acceleration

B_C: Volumetric solutal expansion coefficient

σ: Electrical conductivity

B_0: Magnetic field

T: Fluid temperature

α_{nf}: Nanofluid thermal diffusivity

ρ_f: Fluid density

D_m: Concentration mass diffusivity

C_s: Concentration susceptibility

$(c_p)_{nf}$: Nanofluid specific heat capacity at constant pressure

C: Fluid concentration

Q: Volumetric rate of heat generation

k_m: mean fluid

R: Chemical reaction parameter

T_m: mean fluid.

REFERENCES

[1]. Eiyad, A. N. and Ali, J. C. (2010). Mixed convection flow in a lid-driven inclined square enclosure filled with a nanofluid. *European Journal of Mechanics Fluids,* 29, 472-482.

[2]. Hayata, T. *et al (*2014). MHD flow of nanofluids over an exponentially stretching sheet in a porous medium with convective boundary conditions. *Chin. Phys. B*, 23(5), doi: 10.1088/1674-1056/23/5/054701.

[3]. Khalil, K., Kambiz, V. and Marilyn, L. (2003). Buoyancy-driven heat transfer enhancement in a two-dimensional enclosure utilizing nanofluids. *International Journal of Heat and MassTransfer,* 46, 3639–3653.

[4]. Kuang, C. L. and Angela, V. (2010). Natural convection heat transfer of nanofluids in a vertical cavity: Effects of non-uniform particle diameter and temperature on thermal conductivity. International *Journal of Heat and Fluid flow, 31(2), 236-245.*

[5]. Lee, S. *et al* (1999). Measuring thermal conductivity of fluids containing oxide nanoparticles. *Journal of Heat Transfer*, 121, 280–289.

[6]. Maiga, S. *et al* (2006). Heat transfer enhancement in turbulent tube flow using Al2O3 nanoparticle suspension. *International Journal of Numerical Methods for Heat and Fluid Flow,* 16(3), 275–292.

[7]. Nadeem, S., Ijaz S. and Akbar N. (2013). Nano Particle Analysis for the Steady Blood Flow of Jeffrey Fluid with Stenosis with New Analytical Techniques. *Journal ofcomputational and Theoretical nanoscience*, 10(11), 2751-2765.

[8]. Norfifah, B., Anuar, I. and Ioan P. (2011). Stagnation-point flow over a stretching/shrinking sheet in a nanofluid. *Nanoscale Research Letters © Bachok et al; licensee Springer. 2011,* 10.1186/1556-276X-6-623.

[9]. Noreen, S. A., Beg, A. O., and Khan, H. Z., (2016). Magneto-nanofluid flow with heat transfer past a stretching surface for the new heat flux model using numerical approach. International Journal of Numerical Methods for Heat and Fluid flow, 27(6), 1215-1230.

[10]. Rama, S., Reddy, G. and Ali, C. (2011). Natural Convective Boundary Layer Flow over a Horizontal Plate Embedded in a Porous Medium Saturated with a Nanofluid. *Journal of ModernPhysics,* 2(2), 10.

[11]. Roy, G. *et al* (2004). Investigation of laminar flow and heat transfer in a radial flow cooling system with the use of nanofluids. *Superlattices and Microstructures*, 35, 497–511.

[12]. Syed, T. H., Rizwan, U. H. and Sohail N. (2014). Model-based analysis of micropolar nanofluid flow over a stretching surface. *Eurepean Physical Journal Plus*, 35, 161.

[13]. Sohail, N., and Changhoon, L. (2012). Boundary layer flow of nanofluid over an exponentially stretching surface**.** *Nanoscale Research Letters © Nadeem and Lee; licensee Springer.* 10.1186/1556-276X-7-94.

[14]. Wang, X. Q., Mujumdar, A. S. and Yap, C. (2006). Free Convection Heat Transfer in Horizontal and Vertical Rectangular Cavities Filled with Nanofluids*. International journal on Heat Transfer Conference IHTC-13. Sydney*.

[15]. Xinwei, W. and Xianfan, X. (1999).Thermal Conductivity of Nanoparticle–Fluid Mixture*. Journal of Thermophysics and Heat transfer,* 13, 4.

[16]. Zi, T. Y. (2011). Numerical study of transient buoyancy-driven convective heat transfer of water-based nanofluids in a bottom-heated isosceles triangular enclosure*. International Journal of Heat and Mass Transfer, 54, 526–532.*

[17]. Zoubair, K., Abderrahim, W. and Rachid, S. (2017). Finite Volume Analysis of Free Convection Heat Transfer in a Square Enclosure Filled by Cu-Water Nanofluid Containing Different Shapes of Heating Cylinder. *Journal of Nanofluids*, 6, 1-8.